




Observation of Brillouin optomechanical strong coupling with an 11 GHz mechanical mode

G. ENZIAN,^{1,4} M. SZCZYKULSKA,¹ J. SILVER,² L. DEL BINO,² S. ZHANG,² I. A. WALMSLEY,¹
P. DEL'HAYE,² AND M. R. VANNER^{1,3,*} 

¹Clarendon Laboratory, Department of Physics, University of Oxford, OX1 3PU, UK

²National Physical Laboratory (NPL), Teddington, TW11 0LW, UK

³QOLS, Blackett Laboratory, Imperial College London, London SW7 2BW, UK

⁴e-mail: georg.enzian@physics.ox.ac.uk

*Corresponding author: m.vanner@imperial.ac.uk

Received 4 September 2018; revised 19 November 2018; accepted 26 November 2018 (Doc. ID 344924); published 21 December 2018

Achieving cavity-optomechanical strong coupling with high-frequency phonons provides a rich avenue for quantum technology development, including quantum state transfer, memory, and transduction, as well as enabling several fundamental studies of macroscopic phononic degrees of freedom. Reaching such coupling with GHz mechanical modes, however, has proved challenging, with a prominent hindrance being material- and surface-induced optical absorption in many materials. Here, we circumvent these challenges and report the observation of optomechanical strong coupling to a high-frequency (11 GHz) mechanical mode of a fused-silica whispering-gallery microresonator via the electrostrictive Brillouin interaction. Using an optical heterodyne detection scheme, the anti-Stokes light back-scattered from the resonator is measured, and normal-mode splitting and an avoided crossing are observed in the recorded spectra, providing unambiguous signatures of strong coupling. The optomechanical coupling rate reaches values as high as $G/2\pi = 39$ MHz through the use of an auxiliary pump resonance, where the coupling dominates both optical ($\kappa/2\pi = 3$ MHz) and mechanical ($\gamma_m/2\pi = 21$ MHz) amplitude decay rates. Our findings provide a promising new approach for optical quantum control using light and sound.

Published by The Optical Society under the terms of the [Creative Commons Attribution 4.0 License](https://creativecommons.org/licenses/by/4.0/). Further distribution of this work must maintain attribution to the author(s) and the published article's title, journal citation, and DOI.

<https://doi.org/10.1364/OPTICA.6.000007>

1. INTRODUCTION

Since the 1920s, photon–phonon Brillouin scattering [1–3] has been a subject of intense and diverse study. This nonlinear optical phenomenon has been observed in numerous physical systems, including bulk crystals [4], optical fibers [5,6], integrated devices such as silicon photonic waveguides [7], silica micro-sphere resonators [8], and bulk crystalline resonators [9]. The interaction is now receiving a resurgence of interest and its potential to contribute to both classical- and quantum-information-processing applications has recently been identified. Prominent example applications of Brillouin scattering include optical delay and memory [10,11], coherent waveguide interfacing and filtering [11–13], non-reciprocity [14,15], as well as switching, pulse shaping, and other optical technologies such as fiber Brillouin lasers and amplifiers [16]. Moreover, Brillouin scattering provides a bridge between light and sound and offers an attractive path to coherently connect the microwave and optical domains.

The field of Brillouin scattering is now merging with the rapidly growing field of cavity quantum optomechanics. This merger offers new opportunities to control phononic degrees of freedom at the quantum level to develop new applications, such

as weak-force sensors, and to study the fundamentals of quantum physics at a macroscopic scale. In quantum optomechanics, radiation-pressure is one of the most commonly employed interactions [17], which should be contrasted to electrostriction and photoelasticity, which are central to the physics of Brillouin scattering. It is of vital importance for many optomechanical protocols that a large coupling rate between the electromagnetic and mechanical degrees of freedom be achieved. As in other facets of quantum optics, such as cavity- [18,19] and circuit-quantum electrodynamics [20], it is important to achieve a coupling rate that exceeds the decay rates present in the system. This strong coupling regime has been theoretically studied for an optical cavity field coupling to a mechanical oscillator [21,22] and has now been observed in optomechanical [23] and electromechanical [24] systems where the characteristic Rabi-like splitting of the mechanical power spectral density was demonstrated. It is also important in optomechanics that the coupling rate exceeds the mechanical decoherence rate in order to provide coherent control of the mechanical degree of freedom. This coherent coupling regime has also been observed in both optomechanical [25] and electromechanical systems [26] and enables the exciting prospect

of coherent quantum state transfer between light and mechanical motion.

Brillouin interactions [27–32] have been primarily studied in the stimulated regime that gives a large Stokes-scattering signal; however, very recently anti-Stokes scattering has been gaining more attention, which is relevant for quantum control applications in optomechanics. For instance, laser cooling of a MHz frequency mechanical mode was performed using forward Brillouin scattering [33], similar forward Brillouin scattering was used to suppress Rayleigh scattering [34], thermal anti-Stokes scattering from a silicon waveguide was very recently observed [35], and ultra-long-lived high-frequency phonon modes have been identified in bulk crystalline resonators [9]. Brillouin optomechanics operating in the back-scattering regime unites several favorable properties. Notably, high mechanical frequencies (>10 GHz) enable low thermal occupations to be reached by standard commercial cryogenics; high separability between the optical pump and scattered optical signal can be more easily achieved owing to the large frequency separation and backward scattering direction; and high-bandwidth, multi-wavelength operations can be performed that enable advanced quantum-information processing capabilities. Observing strong coupling for GHz mechanical modes has eluded the optomechanics and Brillouin scattering communities thus far, and entering this regime would enable these united favorable properties to be exploited for optomechanical quantum technology development and advancing the forefront of fundamental quantum science.

Here we report the observation of strong coupling between an optical whispering-gallery mode of a fused-silica microresonator and an 11 GHz mechanical traveling wave via Brillouin anti-Stokes scattering. This is achieved with a continuous-wave pump

at 1550 nm that is resonantly enhanced by an auxiliary cavity mode. The pump field counter-propagates with the mechanical mode and scatters from thermal phonons to create a backward-propagating anti-Stokes optical signal, while Stokes scattering (which can lead to stimulated-Brillouin scattering) is not resonant with the cavity response and thus strongly suppressed. The anti-Stokes signal is then measured using heterodyne detection. As silica has an extremely low optical propagation loss, a strong pump field can be utilized to achieve a coupling rate that far exceeds both optical and mechanical damping rates. Normal-mode splitting and an avoided crossing are observed in the heterodyne spectra, providing unambiguous experimental signatures of strong coupling.

2. RESULTS

Brillouin scattering is a three-wave-mixing process where an optical field interacts with a mechanical traveling wave and generates a frequency-shifted optical signal. There are two sides to this light–matter interaction: electrostriction, where the electric field of light influences the mechanical wave, and photoelasticity, where the mechanical wave modifies the light field. Momentum and energy conservation allow two types of scattering processes: Stokes scattering, where the frequency of the light is downshifted giving rise to optical gain and is commonly observed in the form of stimulated Brillouin scattering or Brillouin lasing; and anti-Stokes scattering, where the light is upshifted giving rise to a mechanical damping mechanism. The phase-matching conditions for the anti-Stokes process utilized in this work are shown in Fig. 1(A). Here, an optical pump field interacts with a counter-propagating mechanical wave generating a back-scattered optical anti-Stokes field. Since the pump and anti-Stokes fields are of a

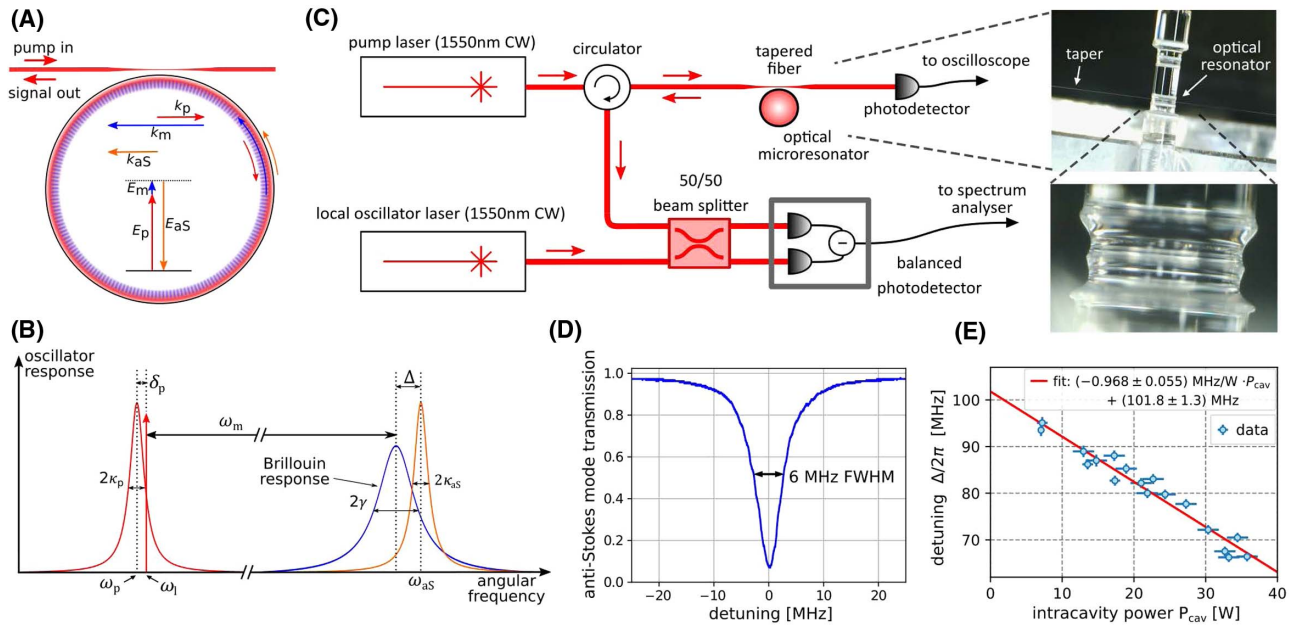


Fig. 1. Experimental platform and setup. (A) Wavevector and energy conservation in Brillouin anti-Stokes scattering. (B) Resonance structure of our Brillouin optomechanical system. Optical (red, orange) and mechanical (blue) modes with their frequencies and decay rates shown. (C) Experimental schematic (left) and optical microscope images of a 700 μm fused-silica microrod whispering-gallery resonator (right). The microresonator is coupled to a tapered optical fiber and driven by a continuous-wave pump laser. Frequency upconverted light backscattered from the resonator is separated by a circulator and measured using optical heterodyne detection and is recorded with a spectrum analyzer. (D) Taper transmission as the laser frequency is scanned across the anti-Stokes cavity resonance. (E) Observed detuning versus intracavity pump power due to optical nonlinearities.

similar frequency, the wavevectors in this back-scatter process are related via $|k_m| \approx 2|k_p| \approx 2|k_{aS}|$, where the subscripts m, p, and aS refer to the mechanical, optical pump, and anti-Stokes modes, respectively (see [Supplement 1](#)).

A. Experimental Setup

We used an optical microresonator that supports two optical whispering-gallery modes spaced by approximately the mechanical frequency [Fig. 1(B)]. A pump laser drives the lower frequency auxiliary cavity mode (with small detuning δ_p) to generate a large intracavity optical field. This field interacts with the mechanical mode, and anti-Stokes light is resonantly scattered into the higher frequency optical mode. As there are only two optical modes that participate, the symmetry between Stokes and anti-Stokes scattering is broken, and the Stokes scattering is strongly suppressed. We label the angular frequency mismatch between the mechanical frequency ω_m , the difference between the anti-Stokes resonance frequency ω_{aS} , and the pump laser frequency ω_L by $\Delta = \omega_{aS} - \omega_L - \omega_m$. Note that the Brillouin frequency does not correspond to the free spectral range of the microresonator. Rather, the two optical modes with the desired frequency spacing are achieved by using different spatial modes that provide significant overlap with the mechanical traveling wave.

The Brillouin frequency shift in bulk silica at 1550 nm is 10.7 GHz, which is obtained from the simple relation $\omega_m \approx 2\omega v/(c/n)$. Here, ω_m is the Brillouin angular frequency shift, v is the speed of sound in silica, c is the speed of light in vacuum, n is the refractive index, and ω is the optical angular frequency. To measure the Brillouin frequency shift, we pumped the higher frequency mode of the optical mode pair and observed Brillouin lasing [8,36,37] using an optical spectrum analyzer. We observed $\omega_m/(2\pi) = (11.01 \pm 0.09)$ GHz, which is consistent with previous stimulated Brillouin scattering measurements in silica microresonators [8] and indicates that electrostriction is the dominant coupling mechanism. The mechanical frequency in the anti-Stokes experiments discussed below must lie very close to this value. We would also like to note here that, unlike in conventional optomechanics, the Brillouin frequency shift has very little dependence on either the optical power or temperature, providing a robust and convenient platform.

A schematic of our telecom-fiber-based experimental setup is shown in [Fig. 1(C)]. We utilize a fused-silica micro-rod resonator [38] (diameter: 700 μm , lateral radius of curvature: ~ 40 μm , free spectral range: 90 GHz) evanescently coupled to a tapered optical fiber. The lower frequency cavity resonance of the pair is driven by a continuous-wave pump laser, and a thermal lock [39] is used, which stabilizes the resonance to the pump laser. The frequency upshifted light backscattered in the resonator is coupled out via the tapered fiber, separated from the pump light by an optical circulator, and mixed with a local oscillator on a 50:50 fiber-beam splitter. We then observe this signal with a balanced detector, implementing optical heterodyne detection with a local oscillator frequency offset of approximately 200 MHz. Heterodyne detection provides a large signal-to-electronic-noise ratio and with the frequency offset allows the shape of the spectra to be easily observed. The heterodyne spectra are recorded using an electrical spectrum analyzer, and the pump power is varied to characterize the Brillouin optomechanical strong coupling features.

The optical damping rates are obtained from separate transmission spectra measurements. Figure 1(D) shows the

cavity mode that enhances the anti-Stokes signal, which has an amplitude decay rate of $\kappa_{aS}/2\pi = 3.0$ MHz. (We will use the convention of amplitude decay rates throughout the article.) Similarly, the pump mode was measured to have an amplitude decay rate of 3.5 MHz. As the mechanical frequency is orders of magnitude larger than the damping rate of the anti-Stokes optical mode, the experiment lies deeply within the resolved sideband regime, i.e., $\omega_m \gg \kappa_{aS}$, which strongly suppresses the Stokes scattering. These optical damping rates have an intrinsic contribution for which the major loss mechanisms have been identified [40] and an external contribution due to the tapered optical fiber coupling (see [Supplement 1](#)).

By fitting to our heterodyne spectra, the mechanical amplitude decay rate was estimated to be $\gamma_m/2\pi = (20.9 \pm 1.6)$ MHz. This value is similar to previous room-temperature in-fiber and bulk silica measurements at 1550 nm [41,42]. We would like to highlight that it has been previously observed that the mechanical damping in such materials is significantly reduced when operating at low temperature, reducing by an order of magnitude at approximately 4 K [43,44].

In our experiment, we observe that the detuning Δ decreases linearly with increasing intracavity pump power [Fig. 1(E)]. We attribute this detuning change to the optical Kerr effect and a possible contribution from the cavity-mode-dependent thermo-refractive effect, which can both cause pump-power-dependent relative frequency shifts between the two optical cavity modes. Concentrating on the former, self- and cross-phase modulations cause power-dependent shifts to the cavity resonances, depending on the mode overlap, and we can model the dependence of the detuning on intracavity power by $\Delta \simeq \Delta_0 - P_{\text{cav}}\omega n_2/(nA')$. Here, Δ is the detuning, Δ_0 is the initial (low power) detuning, ω is the laser angular frequency, n_2 is the nonlinear refractive index, n is the refractive index, A' depends on the difference between the self- and cross-phase modulation terms and has dimensions of an area (see [Supplement 1](#)), and P_{cav} is the intracavity pump power. This purely optical mode overlap is different from the Brillouin optomechanical mode overlap, in that it involves only two (optical) modes, whereas the latter involves a triple overlap integral of one acoustic and two optical modes (see [Supplement 1](#)). From the fit shown in Fig. 1(E), we observe a linear shift of approximately 1 MHz W^{-1} of intracavity power. The measurements in Fig. 1(E) were performed at low power in order to avoid nonlinear loss mechanisms, such as four-wave-mixing parametric oscillation. This detuning measurement was also used as a calibration to determine the intracavity pump power in addition to the transmission measurement described in the Methods section below. We would like to remark that it may be practically possible to engineer a cavity that eliminates the pump-power dependence of the detuning. This could be achieved by exploiting both the self- and cross-phase modulations and using an optical mode structure with an overlap such that the two modes have the same frequency shift as the pump power changes.

B. Model

The Brillouin interaction may be described by a simplified Hamiltonian that couples the two optical modes via the high-frequency mechanical oscillation. Since we are coherently driving the optical pump mode, we approximate its associated field operator by a classical amplitude, which acts to enhance the optomechanical coupling strength. In a frame rotating with the two optical

frequencies, our simplified phenomenological model has the Hamiltonian

$$\frac{H}{\hbar} = G(a_{\text{aS}}^\dagger b + a_{\text{aS}} b^\dagger) - \Delta b^\dagger b.$$

Here, a_{aS} and b are the optical anti-Stokes mode and mechanical field operators, respectively, and $G = g_0|\alpha| \propto \sqrt{P_{\text{cav}}}$ is the intra-cavity-pump-enhanced optomechanical coupling strength. Starting from this Hamiltonian, we compute the system dynamics using quantum Langevin equations. We then utilize optical input–output theory and compute the noise power spectral density of a rotating quadrature of the anti-Stokes field to describe the spectra observed with our heterodyne detection measurements (see Supplement 1). It is important to note here that the present experiment operates in a regime where the acoustic density of states is a quasi-continuum, as the damping rate of each mechanical eigenfrequency component is larger than the mechanical free spectral range. The mechanical field operator b in the simplified model above then describes the linear combination of mechanical eigenfrequency components that contribute to the phase matching. To model the system in this way, we assume that each mechanical frequency component couples equally and, as the optical linewidth is much smaller than the mechanical decay rate, this selects a narrow range of mechanical frequency contributions.

Consistent with our experimental observations detailed in the following section, our model indicates that, for zero detuning, the system undergoes normal-mode splitting when $G > |\kappa_{\text{aS}} - \gamma_{\text{m}}|/2$. We would like to clarify that satisfying this condition does not necessarily demonstrate that strong coupling has been achieved, as the two peaks in the spectra may not be clearly resolved. The conditions of strong coupling are met when the coupling strength G becomes larger than the effective damping rates of the hybrid optical–mechanical modes, i.e., $G > (\kappa_{\text{aS}} + \gamma_{\text{m}})/2$ (see Supplement 1). Under these conditions, a clearly separated avoided crossing may be observed in the spectra, which is an unambiguous signature of strong coupling.

C. Observation of Normal-Mode Splitting and Avoided Crossing

To characterize our Brillouin optomechanical system, we record the heterodyne spectra for a wide range of intracavity pump powers. As P_{cav} increases, the optomechanical coupling rate increases in proportion to $\sqrt{P_{\text{cav}}}$, and simultaneously, the detuning Δ changes linearly with P_{cav} . We then record and fit the heterodyne spectra to obtain estimates of the experimental parameters, aside from the two optical decay rates measured previously, and excellent agreement between our model and the data is found. We would also like to highlight here that the optical resonator does not exhibit optical mode splitting through backscattering from imperfections of the material [45], which enabled us to more easily confirm that the signals observed originate from the Brillouin optomechanical interaction. We plot and analyze the results of this work in terms of the intracavity pump power instead of the input pump power, so that the dependence on pump detuning δ_{p} and taper coupling conditions is removed. This way also provides greater convenience, as the optomechanical coupling rate G and detuning Δ directly depend on P_{cav} . At close to critical coupling, the intracavity power is approximately the input power multiplied by $\mathcal{F}/\pi \approx 4000$, where \mathcal{F} is the cavity finesse.

In Fig. 2, a subset of the observed heterodyne spectra with theoretical fits is plotted. These plots show typical observed spectra, where the detuning varies from large and positive, through zero, to negative, while the optomechanical coupling rate

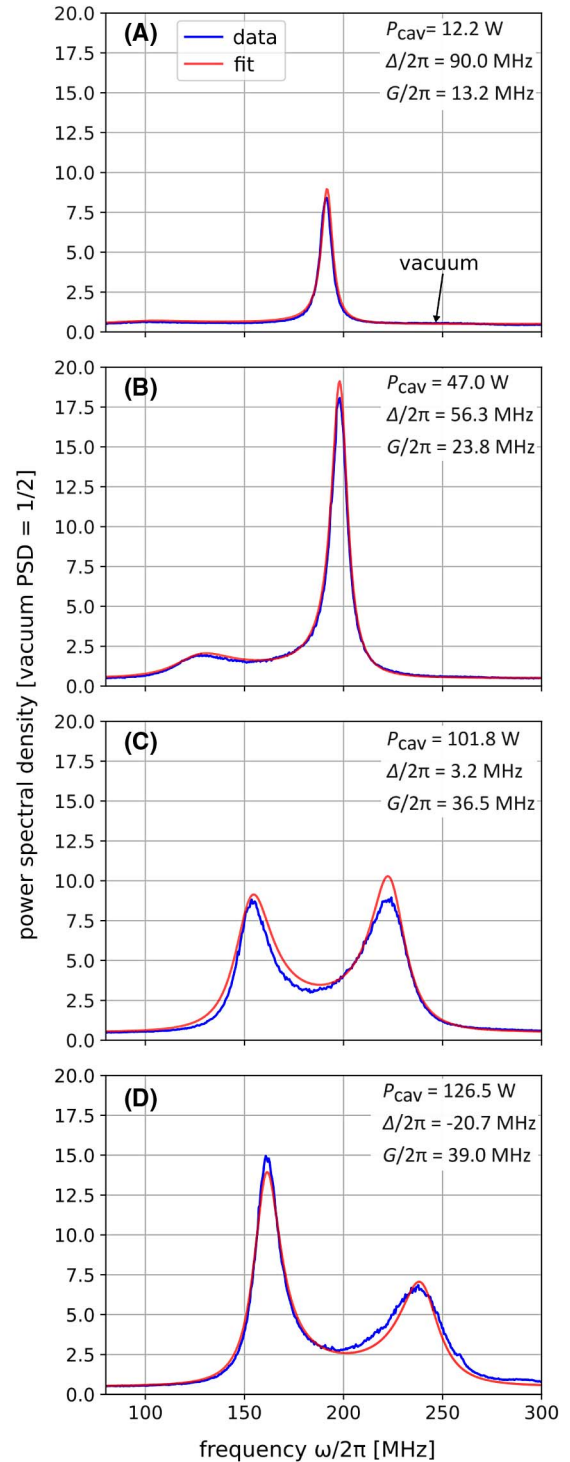


Fig. 2. Observed Brillouin optomechanical anti-Stokes spectra. Power spectral densities of the Brillouin anti-Stokes heterodyne signal (blue) with theoretical fits (red). The spectra are normalized such that a vacuum input corresponds to a value of 1/2. The heterodyne frequency is 190 MHz. As the intracavity pump power is increased from (A) through (D), the detuning decreases, and the coupling rate increases. As the detuning goes through zero, an avoided crossing and normal-mode splitting are observed [see plot (C)].

increases. The spectra comprise a double-peak structure on top of a flat optical vacuum background, where both the widths and center frequencies of the peaks change as the intracavity power changes. For low pump power and large positive detuning, the spectrum contains mainly a single narrow peak [Fig. 2(A)]. As the pump power is increased, the strength of the signal grows, and a second side peak becomes more pronounced [Fig. 2(B)].

As the power is further increased [Fig. 2(C)], two well-separated approximately symmetric peaks are observed. At this power, the coupling rate dominates all damping rates and the detuning in the system. For our particular physical implementation, the detuning passes through zero at this point, and the heights and widths of the two peaks observed are approximately equal. The two peaks in the spectrum correspond to the in-phase and out-of-phase hybrid

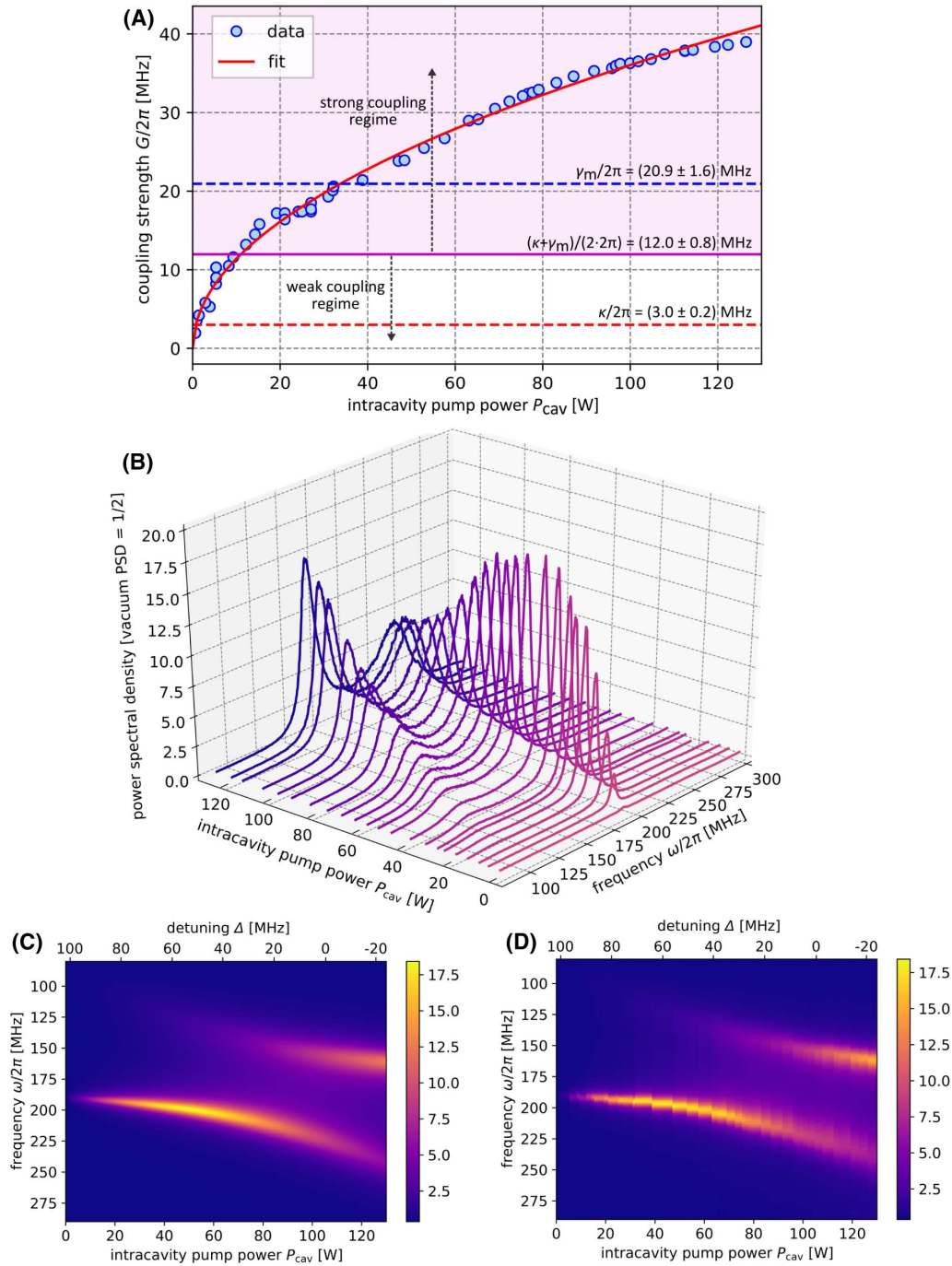


Fig. 3. Brillouin optomechanical strong coupling showing normal-mode splitting and an avoided crossing. (A) Observed optomechanical coupling strength, as determined from the measured spectra, plotted with the intracavity pump power. The expected square-root scaling with the intracavity power is observed and the input-pump powers used were up to 30 mW. The coupling rate achieved far exceeds the damping rates of the system, allowing us to go deeply into the strong coupling regime (shaded purple). (B) Experimentally observed spectra of the anti-Stokes scattered light with varying intracavity pump power. As the power increases, the point of zero detuning is crossed, where an avoided crossing is clearly observed. Theoretically predicted spectra (C) and observed spectra (D), with intracavity pump power. Note the excellent agreement between theory, which includes the power-dependent detuning, and experiment.

optical-mechanical modes, being the eigenstates of the system in the strong coupling regime. The peaks are spaced by $2G$, and their widths are given by the hybrid optical-mechanical damping rates. As the pump power is yet further increased, the peak to the left now becomes stronger and narrower compared to the peak on the right [Fig. 2(D)], and the separation between the two peaks further increases.

Figure 3(A) plots the observed coupling rate with intracavity pump power for our complete set of measurements. The data fit very well to the model, and the predicted scaling $G = g_0|\alpha| \propto \sqrt{P_{\text{cav}}}$ is observed. From a fit to these data, we observe that the coupling rate increases by $(3.605 \pm 0.016)\text{MHz W}^{-1/2}$ of intracavity pump power. To aid comparison, we have overlaid the mechanical amplitude decay rate, the optical amplitude decay rate, and the hybrid-mode damping rate $(\kappa_{\text{as}} + \gamma_{\text{m}})/2$ on this plot. It is seen that the coupling rate surpasses the hybrid-mode damping rate at an intracavity power of less than 10 W, corresponding to a very low input-pump power for these silica systems of only 2.5 mW. With increasing pump power, we can go deeply into the strong coupling regime, achieving a very high coupling rate of approximately 40 MHz, which exceeds the mean of the decay rates by a factor of more than 3.25. Using this fit result for G and knowledge of the resonator geometry, we estimate the underlying Brillouin optomechanical coupling rate to be $g_0/2\pi = (396.5 \pm 1.8)\text{Hz}$, which is consistent with previous theoretical related work on Brillouin Stokes scattering [27–31].

In Fig. 3(B), the observed evolution of the heterodyne spectrum with varying intracavity power is shown. As the intracavity power increases, a second lower frequency peak appears and grows, comes closer in frequency to the first peak, and then the separation increases as the optomechanical coupling rate further increases. This is an avoided crossing, which is an unambiguous signature of strong coupling. In contrast to the more common avoided crossing plots, where the system eigenfrequencies are plotted against the detuning, here, we plot against the intracavity power, which acts as a proxy for detuning because the detuning changes linearly with the intracavity power. Our theoretical model for the heterodyne spectrum with intracavity power is plotted in Fig. 3(C) for our experimental parameters. This model accounts for both the intracavity power-dependent coupling and detuning, and we find excellent agreement with our observations plotted in Fig. 3(D) for comparison. An avoided crossing can be confirmed from our data [Fig. 2 and Figs. 3(B) and 3(D)] by noting that at the point where $\Delta \approx 0$ is reached ($G/2\pi \approx 36\text{ MHz}$, $P_{\text{cav}} \approx 100\text{ W}$), a splitting is observed in the spectrum. Such a

splitting would not be present at $\Delta \approx 0$ if an avoided crossing were not present. For convenience, a list of the main experimental parameters is given in Table 1.

3. CONCLUSION AND OUTLOOK

Using an optically doubly-resonant silica micro-rod resonator, we have experimentally demonstrated Brillouin optomechanical strong coupling for high-frequency phonons (11 GHz) in the back-scattering regime. We observe normal-mode splitting and an avoided crossing in the optical emission spectrum, which give unambiguous signatures of the system operating in the strong coupling regime. This large optomechanical coupling rate was achieved by utilizing silica's electrostriction and very low optical loss. We would like to highlight that our silica system does not suffer from two-photon absorption and strong surface-induced optical losses, which currently preclude many other micro-scale devices, primarily those fabricated from silicon, from entering the strong coupling regime. The Brillouin interaction utilized here additionally provides the advantage that the signal (anti-Stokes) photons are well separated from the pump field due high mechanical frequency and being back-scattered from the pump field. To the best of our knowledge, this platform demonstrates optomechanical strong coupling with the highest mechanical frequency reported thus far.

The strong coupling performance achieved here can be even further improved via several near-, mid-, and longer-term routes. These include: (i) optimizing the choice of cavity mode pairs to simultaneously increase g_0 and reduce the power-dependent detuning; (ii) using higher optical quality factor resonances (quality factors of 10^9 can be routinely fabricated that have an amplitude decay rate $\kappa/2\pi = 100\text{ kHz}$), which will allow lower input pump powers to be employed; (iii) using crystalline materials to reduce the mechanical damping rate [9,46]; (iv) performing the experiments at cryogenic temperatures to reduce thermal occupation and decoherence rate, which also provides the further advantage of reducing the mechanical damping rate [43,44]; and (v) exploring the use of resonators fabricated from other materials with a larger photoelastic coupling such as As_2S_3 . We would also like to highlight at this point that the heating due to intrinsic material absorption in silica for 10 W of intracavity power is expected to be $<100\text{ mK}$ when operating at a base temperature of 4 K.

The united favorable properties of this Brillouin optomechanical system provide a rich avenue to develop a suite of new technologies, including classical and quantum information-processing applications and sensors, and even provide a path for coherent X-band microwave-to-optical conversion. As highlighted above, operating at cryogenic temperatures and using crystalline materials will dramatically reduce the mechanical damping rate. At 4 K, the 11 GHz mechanical mode will have a mean thermal occupation of $\bar{n} \approx 7.6$, and making the conservative assumption that the mechanical damping rate reduces to $\gamma_{\text{m}} \approx 2\text{ MHz}$, the ratio of the mechanical decoherence rate to the mechanical frequency is $\bar{n}\gamma_{\text{m}}/\omega_{\text{m}} = \bar{n}/Q \approx 10^{-3}$, which means there are approximately 10^3 oscillations before decoherence becomes significant. With such reductions to the mechanical damping rate, the mechanical coherence length can exceed the resonator circumference, or equivalently, the mechanical free spectral range can exceed the mechanical decay rate, i.e., $v/\pi D > \gamma_{\text{m}}/2\pi$, where D is the resonator diameter. This parameter regime will be easily entered for resonators of similar size at cryogenic temperatures, and the

Table 1. Microresonator Parameters Achieving Brillouin Optomechanical Strong Coupling

Parameter	Value
Microresonator Diameter	700 μm
$\omega_{\text{as}}/2\pi \approx \omega_{\text{p}}/2\pi$	193 THz ($\lambda \sim 1550\text{ nm}$)
$\kappa/2\pi$	3.0 MHz
$\omega_{\text{m}}/2\pi$	11.0 GHz
$\gamma_{\text{m}}/2\pi$	20.9 MHz
Anti-Stokes quality factor Q_{as}	3.2×10^7
Pump quality factor Q_{p}	$<2.8 \times 10^7$
$\Delta/2\pi$	$-20 \dots +102\text{ MHz}$
$g_0/2\pi$	$(396.5 \pm 1.8)\text{Hz}$
Intracavity pump power P_{cav}	0...126 W
$G/2\pi$	0...39 MHz

mechanical resonances will be resolved. Of the numerous applications and further studies that can be performed in this regime, we would like to highlight that this system can readily enter and explore the quantum-coherent-coupling regime, where $G > \hbar\gamma_m$. The coupling rates achieved so far ($G/2\pi \sim 40$ MHz) should be compared with our conservative estimate for decoherence ($\hbar\gamma_m/2\pi \sim 15$ MHz). Operating in the quantum-coherent-coupling regime allows optomechanical state-swap to be performed. Moreover, the regime allows Rabi-like oscillations with non-classical optical input states, such as single-photon Fock states [25,47,48], to be observed, which is a key outstanding goal in the field. Achieving the strong coupling regime for this system paves the way to pursue this outlook and perform Brillouin-based quantum control of light and sound.

4. METHODS

A. Identifying Cavity-Mode Pairs

In order to find a pair of optical cavity modes that can provide Brillouin optomechanical strong coupling, we first find pairs that give low-threshold Brillouin lasing [8,36] via Stokes scattering where the higher frequency cavity mode is driven. (For the present silica microresonator, this corresponds to ~ 1 mW input power.) We then employ a thermal lock to the lower-frequency mode of the pair and perform heterodyne measurements of the anti-Stokes-scattered light to characterize the system as described in the main text.

B. Determining the Intracavity Power

We determine the intracavity pump power via transmission measurements using the following procedure. For low to moderate intracavity pump powers (< 40 W), the pump-mode linewidth (damping rate) is power independent, as there are no significant optical nonlinearities present, such as four-wave mixing. We then use our knowledge of the pump linewidth and the dimensions of the cavity to compute the finesse of the pump mode $F_p = \Delta\nu_{\text{FSR}}/\Delta\nu_p = c/(\pi n d \Delta\nu_p)$. Here, $\Delta\nu_{\text{FSR}}$ is the cavity's free spectral range, $\Delta\nu_p$ is the pump-mode linewidth, and d is the microresonator diameter. We then compare the observed transmission when thermally locked T to the minimum transmission when on-resonance T_0 to determine the detuning δ_p of the pump laser from resonance. This requires knowledge of the linewidth and cavity coupling conditions, i.e., being under- or over-coupled. Knowing the detuning, total linewidth, finesse, and external cavity coupling rate, we determine the intracavity power via $P_{\text{cav}} = F_p/\pi \cdot P_{\text{in}} \cdot (1 - T)/(1 - \sqrt{T_0})$. Note that this expression is valid for the over-coupled condition, and the sign in the denominator flips for the under-coupled condition.

For higher powers (> 40 W), the above procedure cannot be used due to optical nonlinearities becoming significant and increasing the pump-mode loss. (Note that the signal-mode loss is not increased by these nonlinear effects.) In this regime, we determine the intracavity power via the linear relationship between the detuning, as obtained from a fit to the heterodyne spectra, and the pump-mode intracavity power [cf. Fig. 1(E)]. This method gives consistent results with the above method for the low-power regime.

Funding. Engineering and Physical Sciences Research Council (EPSRC) (EP/K034480/1, EP/N014995); H2020

Marie Skłodowska-Curie Actions (MSCA) (748519, CoLiDR); National Physical Laboratory Strategic Research Programme; H2020 European Research Council (ERC) (756966, MOQUACINO); Royal Academy of Engineering Fellowship.

Acknowledgment. We would like to thank L. Freisem, G. J. Milburn, C. Morrison, K. Mølmer, J. Nunn, J. Price, Y. Henry Wen, and J. Zhang for useful discussions. L. D. B. acknowledges support from EPSRC through the CDT for Applied Photonics. J. S. acknowledges support via a Royal Academy of Engineering Fellowship.

See Supplement 1 for supporting content.

REFERENCES

1. L. Brillouin, "Diffusion de la lumière et des rayons X par un corps transparent homogène-Influence de l'agitation thermique," *Ann. Phys.* **9**, 88–122 (1922).
2. L. I. Mandelstam, "Light scattering by inhomogeneous media," *Zh. Russ. Fiz.-Khim. Ova.* **58**, 381 (1926).
3. C. V. Raman and K. S. Krishnan, "A new type of secondary radiation," *Nature* **121**, 501–502 (1928).
4. R. Y. Chiao, C. H. Townes, and B. P. Stoicheff, "Stimulated Brillouin scattering and coherent generation of intense hypersonic waves," *Phys. Rev. Lett.* **12**, 592–595 (1964).
5. E. P. Ippen and R. H. Stolen, "Stimulated Brillouin scattering in optical fibers," *Appl. Phys. Lett.* **21**, 539–541 (1972).
6. G. P. Agrawal, *Nonlinear Fiber Optics* (Academic, 2013).
7. R. Van Laer, B. Kuyken, D. Van Thourhout, and R. Baets, "Interaction between light and highly confined hypersound in a silicon photonic nanowire," *Nat. Photonics* **9**, 199–203 (2015).
8. M. Tömes and T. Carmon, "Photonic micro-electromechanical systems vibrating at X-band (11-GHz) Rates," *Phys. Rev. Lett.* **102**, 113601 (2009).
9. W. H. Renninger, P. Kharel, R. O. Behunin, and P. T. Rakich, "Bulk crystalline optomechanics," *Nat. Phys.* **14**, 601–607 (2018).
10. Z. Zhu, D. J. Gauthier, and R. W. Boyd, "Stored light in an optical fiber via stimulated Brillouin scattering," *Science* **318**, 1748–1750 (2007).
11. M. Merklein, B. Stiller, K. Vu, S. J. Madden, and B. J. Eggleton, "A chip-integrated coherent photonic-phononic memory," *Nat. Commun.* **8**, 574 (2017).
12. D. Marpaung, B. Morrison, M. Pagani, R. Pant, D.-Y. Choi, B. Luther-Davies, S. J. Madden, and B. J. Eggleton, "Low-power, chip-based stimulated Brillouin scattering microwave photonic filter with ultrahigh selectivity," *Optica* **2**, 76–83 (2015).
13. H. Shin, J. A. Cox, R. Jarecki, A. Starbuck, Z. Wang, and P. T. Rakich, "Control of coherent information via on-chip photonic-phononic emitter-receivers," *Nat. Commun.* **6**, 6427 (2015).
14. C.-H. Dong, Z. Shen, C.-L. Zou, Y.-L. Zhang, W. Fu, and G.-C. Guo, "Brillouin-scattering-induced transparency and non-reciprocal light storage," *Nat. Commun.* **6**, 6193 (2015).
15. Z. Shen, Y.-L. Zhang, Y. Chen, C.-L. Zou, Y.-F. Xiao, X.-B. Zou, F.-W. Sun, G.-C. Guo, and C.-H. Dong, "Experimental realization of optomechanically induced non-reciprocity," *Nat. Photonics* **10**, 657–661 (2016).
16. E. Garmire, "Perspectives on stimulated Brillouin scattering," *New J. Phys.* **19**, 011003 (2017).
17. M. Aspelmeyer, T. J. Kippenberg, and F. Marquardt, "Cavity optomechanics," *Rev. Mod. Phys.* **86**, 1391–1452 (2014).
18. R. J. Thompson, G. Remppe, and H. J. Kimble, "Observation of normal-mode splitting for an atom in an optical cavity," *Phys. Rev. Lett.* **68**, 1132–1135 (1992).
19. J. Raimond, M. Brune, and S. Haroche, "Manipulating quantum entanglement with atoms and photons in a cavity," *Rev. Mod. Phys.* **73**, 565–582 (2001).
20. A. Wallraff, D. I. Schuster, A. Blais, L. Frunzio, R.-S. Huang, J. Majer, S. Kumar, S. M. Girvin, and R. J. Schoelkopf, "Strong coupling of a single photon to a superconducting qubit using circuit quantum electrodynamics," *Nature* **431**, 162–167 (2004).

21. F. Marquardt, J. P. Chen, A. A. Clerk, and S. M. Girvin, "Quantum theory of cavity-assisted sideband cooling of mechanical motion," *Phys. Rev. Lett.* **99**, 093902 (2007).
22. J. M. Dobrindt, I. Wilson-Rae, and T. J. Kippenberg, "Parametric normal-mode splitting in cavity optomechanics," *Phys. Rev. Lett.* **101**, 263602 (2008).
23. S. Groblacher, K. Hammerer, M. R. Vanner, and M. Aspelmeyer, "Observation of strong coupling between a micromechanical resonator and an optical cavity field," *Nature* **460**, 724–727 (2009).
24. J. D. Teufel, D. Li, M. S. Allman, K. Cicak, A. J. Sirois, J. D. Whittaker, and R. W. Simmonds, "Circuit cavity electromechanics in the strong-coupling regime," *Nature* **471**, 204–208 (2011).
25. E. Verhagen, S. Deleglise, S. Weis, A. Schliesser, and T. J. Kippenberg, "Quantum-coherent coupling of a mechanical oscillator to an optical cavity mode," *Nature* **482**, 63–67 (2012).
26. J. D. Teufel, T. Donner, D. Li, J. W. Harlow, M. S. Allman, K. Cicak, A. J. Sirois, J. D. Whittaker, K. W. Lehnert, and R. W. Simmonds, "Sideband cooling of micromechanical motion to the quantum ground state," *Nature* **475**, 359–363 (2011).
27. C. Wolff, M. J. Steel, B. J. Eggleton, and C. G. Poulton, "Stimulated Brillouin scattering in integrated photonic waveguides: forces, scattering mechanisms, and coupled-mode analysis," *Phys. Rev. A* **92**, 013836 (2015).
28. J. E. Sipe and M. J. Steel, "A Hamiltonian treatment of stimulated Brillouin scattering in nanoscale integrated waveguides," *New J. Phys.* **18**, 045004 (2016).
29. R. Van Laer, R. Baets, and D. V. Thourhout, "Unifying Brillouin scattering and cavity optomechanics," *Phys. Rev. A* **93**, 053828 (2016).
30. H. Zoubi and K. Hammerer, "Optomechanical multimode Hamiltonian for nanophotonic waveguides," *Phys. Rev. A* **94**, 053827 (2016).
31. K. P. Huy, J.-C. Beugnot, J.-C. Tchahame, and T. Sylvestre, "Strong coupling between phonons and optical beating in backward Brillouin scattering," *Phys. Rev. A* **94**, 043847 (2016).
32. P. Rakich and F. Marquardt, "Quantum theory of continuum optomechanics," *New J. Phys.* **20**, 045005 (2018).
33. G. Bahl, M. Tames, F. Marquardt, and T. Carmon, "Observation of spontaneous Brillouin cooling," *Nat. Phys.* **8**, 203–207 (2012).
34. S. Kim, J. M. Taylor, and G. Bahl, "Dynamic suppression of Rayleigh light scattering in dielectric resonators," arXiv:1803.02366 (2018).
35. R. Van Laer, C. J. Sarabalis, R. Baets, D. Van Thourhout, and A. H. Safavi-Naeini, "Thermal Brillouin noise observed in silicon optomechanical waveguide," *J. Opt.* **19**, 044002 (2017).
36. I. S. Grudinin, A. B. Matsko, and L. Maleki, "Brillouin lasing with a CaF₂ whispering gallery mode resonator," *Phys. Rev. Lett.* **102**, 043902 (2009).
37. B. Sturman and I. Breunig, "Brillouin lasing in whispering gallery microresonators," *New J. Phys.* **17**, 125006 (2015).
38. P. Del'Haye, S. A. Diddams, and S. B. Papp, "Laser-machined ultrahigh-Q microrod resonators for nonlinear optics," *Appl. Phys. Lett.* **102**, 221119 (2013).
39. T. Carmon, L. Yang, and K. J. Vahala, "Dynamical thermal behavior and thermal self-stability of microcavities," *Opt. Express* **12**, 4742–4750 (2004).
40. M. L. Gorodetsky, A. A. Savchenkov, and V. S. Ilchenko, "Ultimate Q of optical microsphere resonators," *Opt. Lett.* **21**, 453–455 (1996).
41. R. W. Boyd, *Nonlinear Optics*, 3rd ed. (Academic, 2008).
42. M. Nikles, L. Thevenaz, and P. A. Robert, "Brillouin gain spectrum characterization in single-mode optical fibers," *J. Lightwave Technol.* **15**, 1842–1851 (1997).
43. R. Vacher, H. Süssner, and S. Hunklinger, "Brillouin scattering in vitreous silica below 1 K," *Phys. Rev. B* **21**, 5850–5853 (1980).
44. S. Le Floch and P. Cambon, "Study of Brillouin gain spectrum in standard single-mode optical fiber at low temperatures (1.4–370 K) and high hydrostatic pressures (1–250 bars)," *Opt. Commun.* **219**, 395–410 (2003).
45. T. J. Kippenberg, S. M. Spillane, and K. J. Vahala, "Modal coupling in traveling-wave resonators," *Opt. Lett.* **27**, 1669–1671 (2002).
46. J. Hofer, A. Schliesser, and T. J. Kippenberg, "Cavity optomechanics with ultrahigh-Q crystalline microresonators," *Phys. Rev. A* **82**, 031804 (2010).
47. U. Akram, N. Kiesel, M. Aspelmeyer, and G. J. Milburn, "Single-photon opto-mechanics in the strong coupling regime," *New J. Phys.* **12**, 083030 (2010).
48. F. Khalili, S. Danilishin, H. Miao, H. Müller-Ebhardt, H. Yang, and Y. Chen, "Preparing a mechanical oscillator in non-Gaussian quantum states," *Phys. Rev. Lett.* **105**, 070403 (2010).